Catalysis Today 164 (2011) 246–250

Contents lists available at ScienceDirect

Catalysis Today

journal homepage: www.elsevier.com/locate/cattod

Ultrasonic-assisted fabrication of $LaNiO_x$ composite oxide nanotubes and application to the steam reforming of ethanol

Siao-Wun Liu [a], Jyong-Yue Liu [a], Ying-Huei Liu [a], Yu-Hsung Huang [a], Chuin-Tih Yeh [b,c], Chen-Bin Wang [a,*]

[a] Department of Applied Chemistry and Materials Science, Chung Cheng Institute of Technology, National Defense University, Tahsi, Taoyuan 33509, Taiwan, ROC
[b] Department of Chemical Engineering and Materials Science, Yuan Ze University Chungli, Taoyuan, Taiwan, ROC
[c] Fuel Cell Center, Yuan Ze University Chungli, Taoyuan, Taiwan, ROC

ARTICLE INFO

Article history:
Available online 14 November 2010

Keywords:
Steam reforming of ethanol (SRE)
Composite oxide
Nanotubes

ABSTRACT

A novel ultrasonic-assisted route for the preparation of $LaNiO_x$ composite oxide nanotubes was developed in this study. A nickel–lanthanum composite oxide with a 1:1 molar ratio was prepared by the co-precipitation–oxidation method (PO) and assisted with 240 W ultrasonic irradiation (assigned as U-$LaNiO_x$). The composite oxide nanorods were synthesized by the co-precipitation–oxidation method (assigned as $LaNiO_x$) without ultrasonic irradiation. Both samples were characterized by X-ray diffraction (XRD), transmission electron microscopy (TEM), BET and temperature-programmed reduction (TPR). Catalytic activity toward the steam reforming of ethanol (SRE) was tested in the temperature range of 300–450 °C in a fixed-bed reactor. The results indicated that U-$LaNiO_x$ nanotubes have better activity which enables 100% ethanol conversion at 325 °C; while a conversion temperature of above 425 °C is required for the $LaNiO_x$ nanorods. The distribution of CO is minor for both samples. This demonstrated that the water gas shift reaction (WGSR) is an important side-reaction in the SRE reaction over both composite oxides to produce H_2 and CO_2.

1. Introduction

With increasingly rapid developments in industry and technology, energy requirements have become of utmost importance. The source of most of our energy is fossil fuel [1]; however, it is not only a non-renewable energy source, but also it creates serious environmental problems, i.e., green house gases and air pollution. Fossil fuel must be replaced by clean and efficient alternative energies. Of these new energies, hydrogen seems to be the ideal energy [2]. It can be used in fuel cells to generate electricity, its only emission is water, and its use would reduce the demand for imported fossil fuels and result in less air pollution [3,4]. The reforming of bio-ethanol provides a promising method for hydrogen production from a renewable resource [1,5]. Moreover, a high yield of hydrogen can be obtained from the steam reforming of ethanol (SRE) [1,5–11].

Nickel is used as an active catalyst in industry, as it has high C–C bond-breaking activity and a relatively low cost [3,7,12,13]. It also has been used in the steam reforming of ethanol, but the Ni catalyst suffers severe deactivation caused by the sintering of nickel and the heavy coke deposition during the steam reforming process [14]. Recent studies have shown that carbon deposition on Ni catalysts for the steam reforming of ethanol can be strongly suppressed by adding promoters such as La and Cu [15]. Fatsikostas et al. [16,17] showed that Ni/La_2O_3 exhibited high activity and stability in the steam reforming of ethanol to hydrogen. This was attributed to the formation of lanthanum oxycarbonate species ($La_2O_2CO_3$), which forms due to the adsorption of CO_2 on La_2O_3 and reacts with the surface carbon deposited during the reaction, thus preventing deactivation. Salavati-Niasari et al. [18,19] reported about the ultrasonic chemistry in the synthesis of nanoparticles, nanotubes were applied. They synthesized successfully $Dy_2(CO_3)_3$ nanoparticles and $Dy(OH)_3$ nanotubes.

The aim of this work was to prepare and then study the effect of the application of ultrasonic-assisted nickel–lanthanum composite oxide nanotubes on the steam reforming of ethanol. The expectation was that the catalytic activity and stability against coke deposition of $LaNiO_x$ catalysts on the SRE reaction could be enhanced. The characterization of the catalysts was analyzed by X-ray diffraction (XRD), temperature-programmed reduction (TPR) and TEM.

2. Experimental

2.1. Preparation of catalyst

A nickel–lanthanum composite oxide, U-$LaNiO_x$, with a 1:1 molar ratio, was prepared by the co-precipitation–oxidation

* Corresponding author.
E-mail addresses: chenbinwang@gmail.com, chenbin@ccit.edu.tw (C.-B. Wang).

0920-5861/$ – see front matter © 2010 Elsevier B.V. All rights reserved.
doi:10.1016/j.cattod.2010.10.017

method (PO) and assisted with ultrasonic irradiation. The co-precipitation–oxidation method involved mixing nickel and lanthanum precursor solutions. Initially, an aqueous solution of nickel nitrate [$Ni(NO_3)_2{\cdot}6H_2O$, Showa] and lanthanum nitrate [$La(NO_3)_3{\cdot}6H_2O$, Showa] was mixed and stirred, while a 3.2 M NaOH solution was added dropwise to produce precipitation; a 12% NaOCl solution was then added dropwise to oxidize the precipitant. All processes were irradiated under ultrasonic (240 W). Another sample, $LaNiO_x$, with a 1:1 molar ratio was also prepared with the PO method without ultrasonic irradiation. Then, the suspension was filtered and washed seven times with DI water. Finally, it was dried at 110 °C overnight.

2.2. Characterization of catalyst

X-ray diffraction (XRD) measurements were performed using a MAC Science MXP18 diffractometer with Cu $K_{\alpha1}$ radiation ($\lambda = 1.5405$ Å) at 40 kV and 30 mA. The reduction behavior of the $LaNiO_x$ composite oxides was studied by temperature-programmed reduction (TPR). About 50 mg of the sample was heated in a flow of 10% H_2/N_2 gas at a flow rate of 10 ml min^{-1}. During TPR, the temperature increased at a rate of 7 °C min^{-1} from room temperature to 900 °C. Transmission electron micrographs (TEM) were taken on a PHILIPS (CM-200) microscope at an accelerating voltage of 200 kV. The samples for TEM were prepared by ultrasonic dispersion of the powder products in ethanol, and then deposited and dried on a holey carbon film on a copper grid.

2.3. Evaluation of catalytic activity

The catalytic activities of the composite oxides towards the SRE reaction were performed at atmospheric pressure in a fixed-bed flow reactor. Catalyst in the amount of 100 mg was placed in a 4 mm i.d. quartz tubular reactor and held by glass–wool plugs. The feed of the reactants comprised a gaseous mixture of ethanol (EtOH), H_2O and Ar. The composition of the reactant mixture (H_2O/EtOH/Ar = 37/3/60 vol.%) was controlled by an Ar stream flow (22 ml min^{-1}) through the saturator (maintained at 120 °C) containing EtOH and H_2O. The gas hourly space velocity (GHSV) was maintained at 22,000 h^{-1} and the H_2O/EtOH molar ratio was 13. Prior to the reaction, the sample was activated by reduction with hydrogen at 200 °C for 3 h. The SRE activity was tested stepwise by increasing the temperature from 300 to 450 °C. The analysis of the reactants and all the reaction products was carried out online by gas chromatography with columns of Porapak Q and Molecular Sieve 5A to separate.

3. Results and discussion

Fig. 1 shows the XRD profiles of the U-$LaNiO_x$ and $LaNiO_x$ samples. Both samples had similar peaks, which matched the JCPDS 83-2034 file that identifies lanthanum hydroxide, $La(OH)_3$, with a hexagonal structure; but, the absence of nickel-species may have been because the nickel particles were too small (probably less than 5 nm) to be detected [20] or had an amorphous structure.

Fig. 2 shows the TPR profiles of the U-$LaNiO_x$ and $LaNiO_x$ samples. The U-$LaNiO_x$ sample [Fig. 2(A)] had four main reduction peaks around 197 °C (T_{r1}), 323 °C (T_{r2}), 382 °C (T_{r3}) and 590 °C (T_{r4}). According to our previous study and literature reports [21–23], we assigned these peaks to the reduction of continuous reductive nickel oxyhydroxide, NiO(OH) (T_{r1} and T_{r2}), $La(OH)CO_3$ (T_{r3}) and $La_2O_2CO_3$ (T_{r4}) as shown in the following equations:

$$2NiO(OH) + H_2 \rightarrow 2NiO + 2H_2O \quad (1)$$

$$NiO + H_2 \rightarrow Ni + H_2O \quad (2)$$

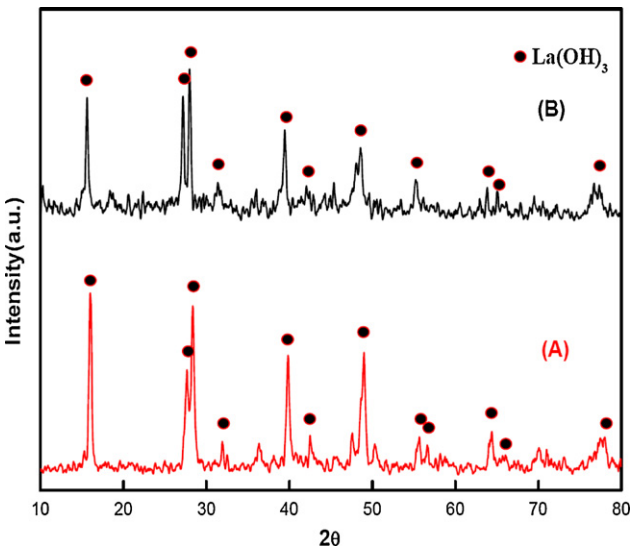

Fig. 1. XRD profiles of nickel lanthanum oxides: (A) U-$LaNiO_x$ and (B) $LaNiO_x$.

$$2La(OH)CO_3 + 2H_2 \rightarrow La_2O_3 + 3H_2O + 2CO \quad (3)$$

$$La_2O_2CO_3 + H_2 \rightarrow La_2O_3 + H_2O + CO \quad (4)$$

Although the XRD diffraction patterns did not observe the amorphous phases of NiO(OH), $La(OH)CO_3$ and $La_2O_2CO_3$ for the U-$LaNiO_x$ and $LaNiO_x$ samples, another two main broad reduction peaks were observed: one at 382 °C of $LaCO_3OH$ reduced to La_2O_3; and the other at 590 °C of $La_2O_2CO_3$ reduced to La_2O_3, because $La(OH)_3$ is very sensitive to atmospheric conditions [24,25]. Under normal conditions of temperature and pressure, it tends to absorb moisture and CO_2 in air [26], and then form $LaCO_3OH$ and $La_2O_2CO_3$ at a high temperature. The TPR profile of the $LaNiO_x$ sample [Fig. 2(B)] was very similar to the U-$LaNiO_x$ sample, but the first reduction peak temperature was lower. This phenomenon was due to the ultrasonic-assisted preparation of the catalyst which enhanced the interaction between the nickel and lanthanum.

Fig. 3 shows the TEM micrographs of the U-$LaNiO_x$ [Fig. 1(A)] and $LaNiO_x$ [Fig. 1(B)] composite oxides. It revealed the presence of nanotubes and nanorods in these composite oxides. Comparing with the pure LaO_x and NiO_x samples showed that the distribution of nanotubes/nanorods came from the $La(OH)_3$ that formed under

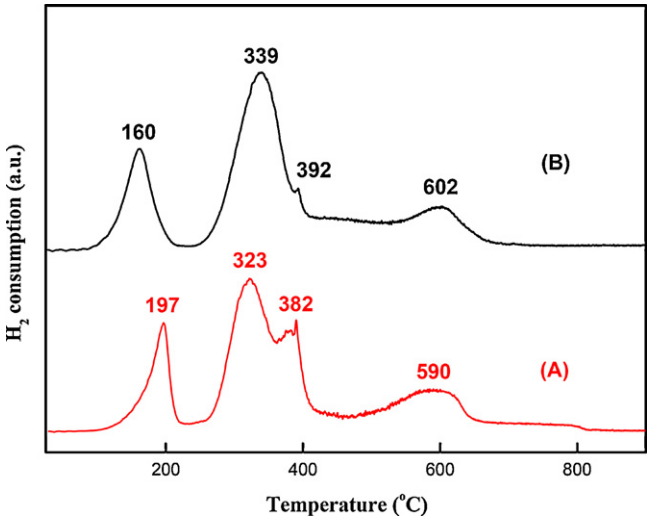

Fig. 2. TPR profiles of nickel lanthanum oxides: (A) U-$LaNiO_x$ and (B) $LaNiO_x$.

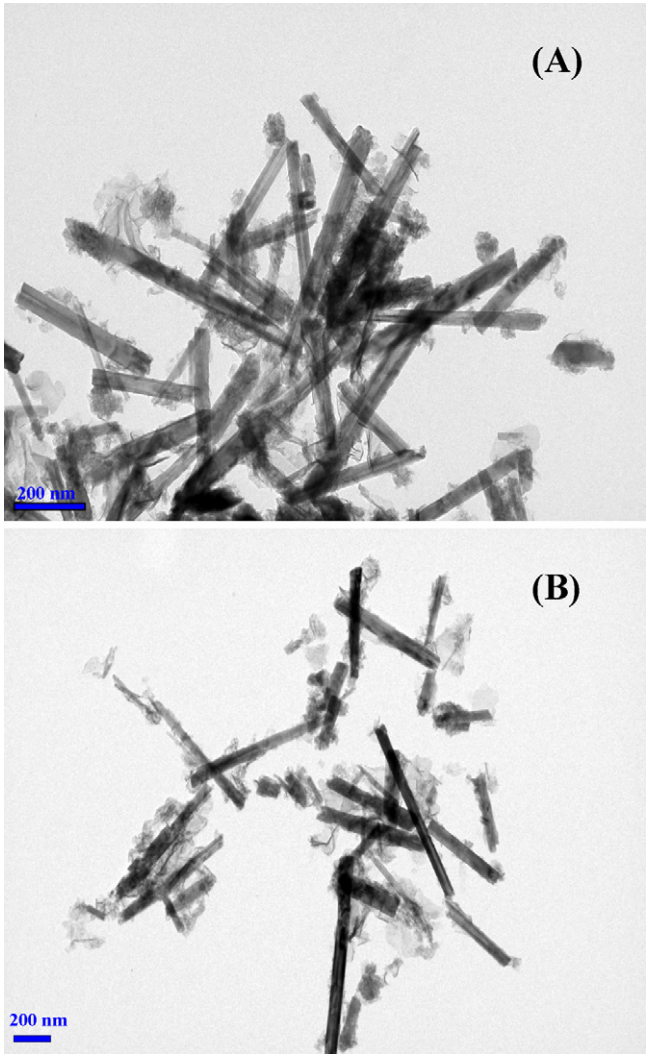

Fig. 3. TEM images of nickel lanthanum oxides: (A) U-LaNiO$_x$ and (B) LaNiO$_x$.

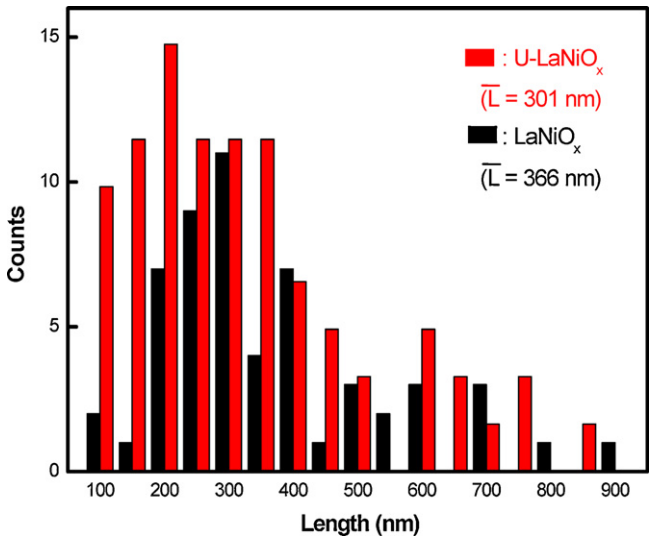

Fig. 4. Length of nanotubes and/or nanorods distribution on U-LaNiO$_x$ and LaNiO$_x$ catalysts.

ultrasonic irradiation and was catalyzed by nickel. Mazloumia et al. [27] ascribed the formation of rare earth hydroxide nanotubes to the existence of lamellar structures. Fig. 4 shows the length of nanotubes and/or nanorods distribution on U-LaNiO$_x$ and LaNiO$_x$ catalysts and presences with ranging from 100 to 900 nm. The average length as determined from TEM images were 301 and 366 nm, respectively for U-LaNiO$_x$ and LaNiO$_x$ catalysts. Fig. 5 shows HR-TEM image and EDX of U-LaNiO$_x$ catalyst. Apparently, the distribution of components on different regions is different. The component of the inner wall of nanotube is mainly the La(OH)$_3$, the component of nickel exists on the knot adjacent to the outside of nanotubes. Apparently, the role of nickel acts as a catalyst to promote the formation of nanotubes under ultrasonic irradiation. Otherwise, only a few nanotubes dispersed in the nanorods were observed for the LaNiO$_x$ sample.

Figs. 6 and 7 show a comparison of the SRE reaction over the LaNiO$_x$ (Fig. 6) and U-LaNiO$_x$ (Fig. 7) composite oxides. There were significant differences in catalyst activity due to the different methods. Clearly, the U-LaNiO$_x$ nanotubes had better activity than the LaNiO$_x$ nanorods. The results indicated that the ethanol conversion approached completion around 325 °C for the U-LaNiO$_x$ sample, while a temperature of 425 °C was required for the LaNiO$_x$ sample to complete conversion. At lower temperatures, the main reaction was the dehydrogenation of ethanol to acetaldehyde. As the temperatures rose, the major reaction proceeded with acetaldehyde decomposition into methane and CO. This indicated that the nickel-species had a stronger capacity for breaking the C–C bond in the reforming of ethanol [1,4,12,13,20]. When comparing the effect of temperature on the decomposition of acetaldehyde (D_T), the easy cracking of acetaldehyde promoted an increase in the hydrogen yield (Y_{H2}). Nevertheless, the promoting effect of the U-LaNiO$_x$ sample was more pronounced than that of the LaNiO$_x$ sample. The

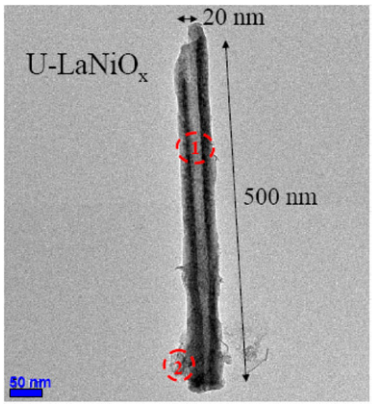

Element	Weight (%)		Atomic (%)	
	Region 1	Region 2	Region 1	Region 2
O	40.45	57.17	85.50	88.04
Ni	0.00	18.00	0.00	7.55
La	59.55	24.83	14.50	4.41
Totals	100.00		100.00	

Fig. 5. HR-TEM image and EDX of U-LaNiO$_x$ catalyst.

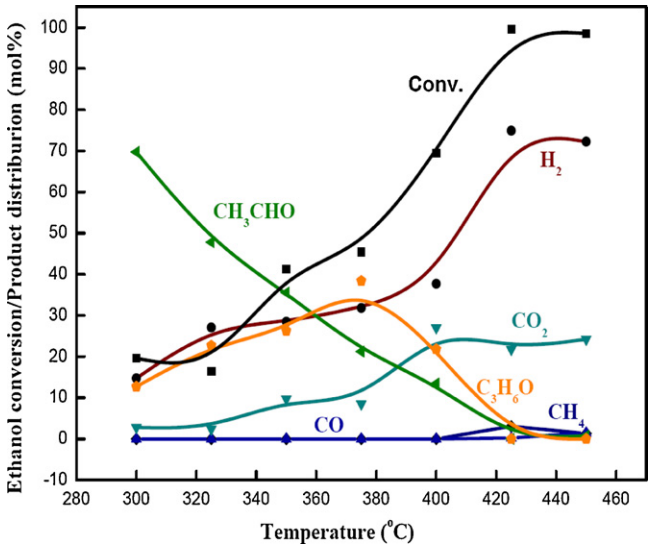

Fig. 6. Catalytic performance in the SRE reaction over $LaNiO_x$ catalyst.

D_T of the U-$LaNiO_x$ sample approached 325 °C, and above 375 °C for the $LaNiO_x$ sample. Comparing with the results of Homs et al. [28] showed that the distribution of hydrogen was higher at this low temperature. Also, the distribution of CO was minor (<1%) for both samples and was lower than that reported in the literatures (CO > 5%) [15,29]. This demonstrated that the water gas shift reaction (WGSR) was an important side-reaction in the SRE reaction over both the U-$LaNiO_x$ and $LaNiO_x$ composite oxides used to produce H_2 and CO_2:

$$CO + H_2O \rightarrow H_2 + CO_2 \quad (5)$$

Amounts of C_2 (CH_3CHO) and C_3 (CH_3COCH_3) products distribution on the $LaNiO_x$ sample below 400 °C indicated that the structure of the nanorods initiated the aldol condensation of ethanol. The concentration of hydrogen increased abruptly as temperatures approached 400 °C, whereas the concentration of both C_2 and C_3 products decreased gradually. This phenomenon indicated that the steam reforming of acetaldehyde and acetone [30] were thermodynamically feasible under high temperatures:

$$CH_3CHO + 3H_2O \rightarrow 5H_2 + 2CO_2 \quad (6)$$

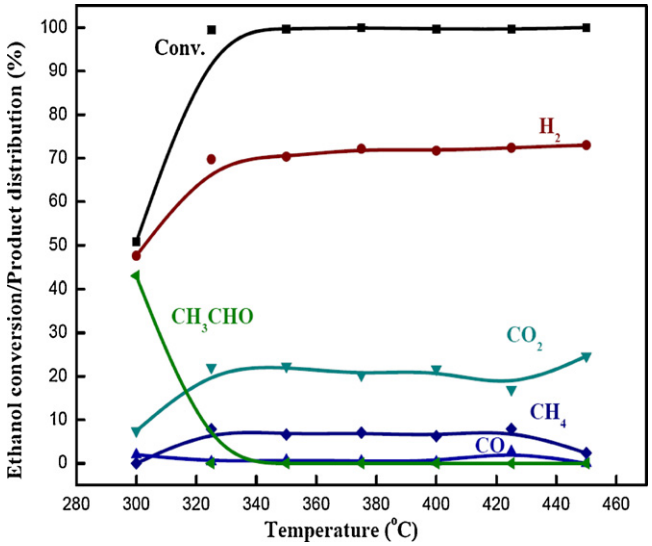

Fig. 7. Catalytic performances in the SRE reaction over U-$LaNiO_x$ catalyst.

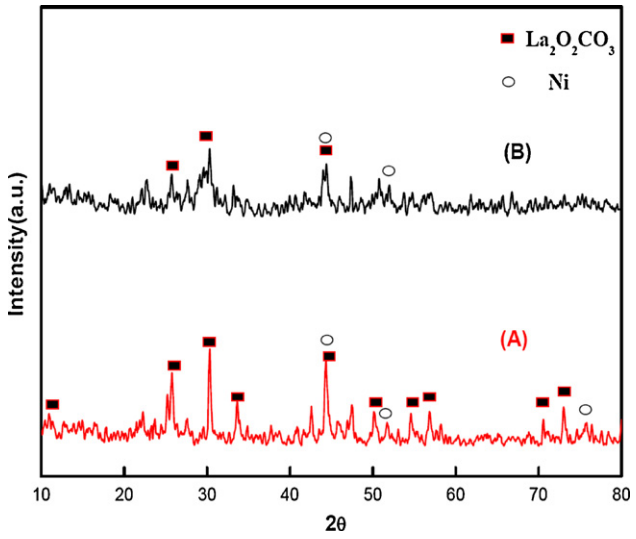

Fig. 8. XRD profiles of used nickel lanthanum oxides: (A) U-$LaNiO_x$ and (B) $LaNiO_x$.

$$CH_3COCH_3 + 5H_2O \rightarrow 8H_2 + 3CO_2 \quad (7)$$

Fig. 8 shows the XRD profiles of the U-$LaNiO_x$ and $LaNiO_x$ samples after the SRE reaction. A comparison with the fresh samples (see Fig. 1) showed clear differences before and after the reaction. There was several diffraction peaks observed for $La_2O_2CO_3$ which formed due to the adsorption of CO_2 on La_2O_3; while no diffraction peaks of La_2O_3 were observed. Fig. 9 shows the TPR profiles of the U-$LaNiO_x$ and $LaNiO_x$ samples after the SRE reaction. The reduction peaks of the two samples below 400 °C were NiO_x signal. Above 400 °C, one sharp reduction peak was observed at 652 °C on U-$LaNiO_x$ [see Fig. 9(A)] that was $La_2O_2CO_3$ reduced to La_2O_3 as follows:

$$La_2O_2CO_3 + H_2 \rightarrow La_2O_3 + CO + H_2O \quad (8)$$

But in Fig. 9(B), $LaNiO_x$ had a broad reduction peak which meant the two peaks covered each other: one was the deposited coke with a different degree of graphitization on the Ni particles [31,32]; and the other was the $La_2O_2CO_3$ reduction signal because LaO_x on Ni particles had the ability to remove carbon deposition in the U-$LaNiO_x$ catalyst.

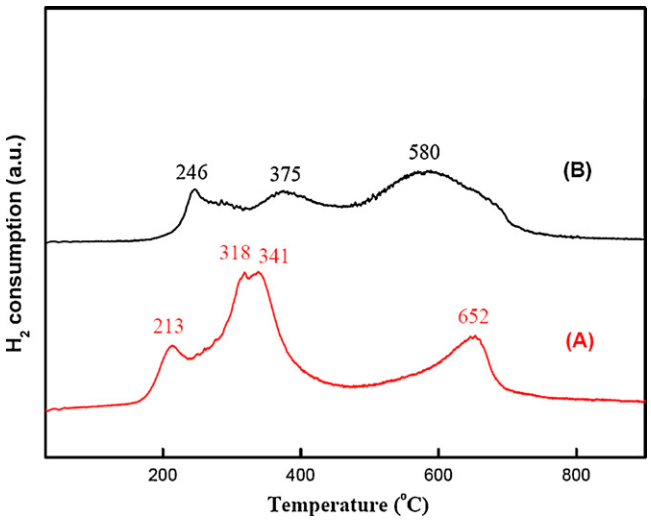

Fig. 9. TPR profiles of used nickel lanthanum oxides: (A) U-$LaNiO_x$ and (B) $LaNiO_x$.

4. Conclusions

In this study, a fabrication process for nickel–lanthanum composite oxide nanotubes with ultrasonic irradiation was developed. The ethanol conversion was almost 100% around 325 °C for the U-$LaNiO_x$ nanotubes, while a temperature of 425 °C was required for the $LaNiO_x$ nanorods. The distribution of CO was minor for both samples, which demonstrated that the WGSR was an important side-reaction in the SRE reaction over both composite oxides to produce H_2 and CO_2.

Acknowledgement

We are pleased to acknowledge the financial support for this study by the National Science Council of the Republic of China under contract numbers of NSC 99-2113-M-606-001-MY3 and 97-2627-M-606-001.

References

[1] M. Ni, D.Y.C. Leung, M.K.H. Leung, Int. J. Hydrogen Energy 32 (2007) 3238.
[2] M.C. Sánchez-Sánchez, R.M. Navarro, J.L.G. Fierro, Catal. Today 129 (2007) 336.
[3] J. Llorca, N. Homs, J. Sales, P.R. de la Piscina, J. Catal. 222 (2004) 470.
[4] J. Sun, X. Qiu, F. Wu, W. Zhu, Int. J. Hydrogen Energy 30 (2005) 437.
[5] H. Muroyama, R. Nakase, T. Matsui, K. Eguchi, Int. J. Hydrogen Energy 35 (2010) 1575.
[6] J. Llorca, N. Homs, J. Sales, P.R. de la Piscina, J. Catal. 209 (2002) 306.
[7] A.N. Fatsikostas, X.E. Verykios, J. Catal. 225 (2004) 439.
[8] P.K. Cheekatamarla, C.M. Finnerty, J. Power Sources 160 (2006) 490.
[9] F. Frusteri, S. Freni, L. Spadaro, V. Chiodo, G. Bonura, S. Donato, Catal. Commun. 5 (2004) 611.
[10] C.B. Wang, C.C. Lee, J.L. Bi, J.Y. Siang, J.Y. Liu, C.T. Yeh, Catal. Today 146 (2009) 76.
[11] J.Y. Siang, C.C. Lee, C.H. Wang, W.T. Wang, C.Y. Deng, C.T. Yeh, C.B. Wang, Int. J. Hydrogen Energy 35 (2010) 3456.
[12] F. Frusteri, S. Freni, V. Chiodo, L. Spadaro, O. Di Blasi, G. Bonura, S. Cavallaro, Appl. Catal. A 270 (2004) 1.
[13] B. Prakash, K. Deepak, Int. J. Hydrogen Energy 32 (2007) 969.
[14] F. Wang, Y. Li, W.J. Cai, E. Zhan, X. Mu, W.J. Shen, Catal. Today 146 (2009) 31.
[15] J.W.C. Liberatori, R.U. Ribeiro, D. Zanchet, F.B. Noronha, J.M.C. Bueno, Appl. Catal. A 327 (2007) 197.
[16] A.N. Fatsikostas, D.I. Kondarides, X.E. Verykios, Chem. Commun. (2001) 851.
[17] A.N. Fatsikostas, D.I. Kondarides, X.E. Verykios, Catal. Today 75 (2002) 145.
[18] M. Salavati-Niasari, J. Javidi, F. Davar, Sonochemistry 17 (2010) 870.
[19] M. Salavati-Niasari, J. Javidi, F. Davar, A.A. Fazl, J. Alloy Compd. 503 (2010) 500.
[20] B.C. Zhang, X.L. Tang, Y. Li, W.J. Cai, Y. Xu, W.J. Shen, Catal. Commun. 7 (2006) 367.
[21] C.B. Wang, G.Y. Gau, S.J. Gau, C.W. Tang, J.L. Bi, Catal. Lett. 101 (2005) 241.
[22] S.G. Germá, M. Fanor, J.M. Tatibouët, B. Joël, B.D. Catherine, Catal. Today 133/135 (2008) 200.
[23] T.L. Lai, Y.Y. Shu, G.L. Huang, C.C. Lee, C.B. Wang, J. Alloy Compd. 450 (2008) 318.
[24] I. Djerdj, G. Garnweitner, D.S. Su, M. Niederberger, Solid State Chem. 180 (2007) 2154.
[25] Q. Shu, J. Liu, J. Zhang, M. Zhang, J. Univ. Sci. Technol., Beijing 13 (2006) 456.
[26] A. Neumann, D. Walter, Thermochim. Acta 445 (2006) 200.
[27] M. Mazloumia, N. Shahcheraghi, A. Kajbafvala, S. Zanganeh, A. Lak, M.S. Mohajerani, S.K. Sadrnezhaad, J. Alloy Compd. 473 (2009) 283.
[28] N. Homs, J. Llorca, P.R. de la Piscina, Catal. Today 116 (2006) 361.
[29] A.J. Vizcaino, A. Carrero, J.A. Calles, Int. J. Hydrogen Energy 32 (2007) 1450.
[30] X. Hu, G.X. Lu, Appl. Catal. B 88 (2009) 376.
[31] S. Freni, S. Carvallaro, N. Mondello, L. Spadaro, F. Frusteri, Catal. Commun. 4 (2003) 259.
[32] L. Zhang, W. Li, J. Liu, C. Guo, Y. Wang, J. Zhang, Fuel 88 (2009) 51.